Development 135, 387-399 (2008) doi:10.1242/dev.006098

The zebrafish mutant *lbk/vam6* resembles human multisystemic disorders caused by aberrant trafficking of endosomal vesicles

Helia B. Schonthaler[1,2,*], Valerie C. Fleisch[1,2], Oliver Biehlmaier[2], Yuri Makhankov[1], Oliver Rinner[1], Ronja Bahadori[1], Robert Geisler[3], Heinz Schwarz[3], Stephan C. F. Neuhauss[1,2,†,‡] and Ralf Dahm[3,†,§]

The trafficking of intracellular vesicles is essential for a number of cellular processes and defects in this process have been implicated in a wide range of human diseases. We identify the zebrafish mutant *lbk* as a novel model for such disorders. *lbk* displays hypopigmentation of skin melanocytes and the retinal pigment epithelium (RPE), an absence of iridophore reflections, defects in internal organs (liver, intestine) as well as functional defects in vision and the innate immune system (macrophages). Positional cloning, an allele screen, rescue experiments and morpholino knock-down reveal a mutation in the zebrafish orthologue of the *vam6/vps39* gene. Vam6p is part of the HOPS complex, which is essential for vesicle tethering and fusion. Affected cells in the *lbk* RPE, liver, intestine and macrophages display increased numbers and enlarged intracellular vesicles. Physiological and behavioural analyses reveal severe defects in visual ability in *lbk* mutants. The present study provides the first phenotypic description of a lack of *vam6* gene function in a multicellular organism. *lbk* shares many of the characteristics of human diseases and suggests a novel disease gene for pathologies associated with defective vesicle transport, including the arthrogryposis-renal dysfunction-cholestasis (ARC) syndrome, the Hermansky-Pudlak syndrome, the Chediak-Higashi syndrome and the Griscelli syndrome.

KEY WORDS: Zebrafish development, Eye, Vision, Pigmentation, Liver, Vesicle trafficking, Lysosomes and lysosome-related organelles, Vam6p/Vps39

INTRODUCTION

Vesicle trafficking is essential for a wide range of cellular processes and defects in vesicle trafficking have been shown to underlie various human diseases. In the arthrogryposis-renal dysfunction-cholestasis (ARC) syndrome, for example, mutations in the *VPS33B* gene lead to a dysregulation of vesicle fusion, including lysosomes and late stage endosomes (Gissen et al., 2004) (OMIM #208085). Similarly, the Chediak-Higashi syndrome (CHS), Hermansky-Pudlak syndrome (HPS) and Griscelli syndrome (GS) have been linked to a number of proteins involved in the formation, trafficking and fusion of lysosome and lysosome-related organelles [OMIM #214500 (CHS), #203300 (HPS), #214450 (GS1), #607624 (GS2), #609227 (GS3)]. These inherited human diseases are associated with hypopigmentation, prolonged bleeding and immunological defects. It has also been reported that affected individuals display visual defects, including photophobia, strabismus and nystagmus. Although mutations in several genes have been linked to these diseases, it has not yet been possible to identify the molecular defects in all cases.

Lysosome-related organelles are cell type-specific organelles that share several physiological properties with lysosomes (Raposo and Marks, 2002). They include organelles, such as melanosomes in skin and RPE melanocytes, lamellar bodies in type II lung epithelial cells, dense granules in platelets and MHC class II compartments in antigen-presenting cells, and cytotoxic granules of lymphocytes. Tethering and docking of lysosomes and lysosome-related organelles depends on the HOPS complex (homotypic fusion and vacuole protein sorting complex). This complex interacts with both SNAREs and Ypt7p/Rab7 (Collins et al., 2005; Price et al., 2000a; Price et al., 2000b; Sato et al., 2000; Wurmser et al., 2000) and is required for SNARE complex assembly (Stroupe et al., 2006). Furthermore, the HOPS complex seems to be important for early-late endosome transition in the Rab-conversion model in mammalian cells (Rink et al., 2005). The HOPS complex comprises the class C Vps protein Vam5p/Vps33p, the protein defective in ARC syndrome; the class C proteins Vam1p/Vps11p, Vam9p/Vps16p and Vam8p/Vps18p; and two class B Vps proteins, Vam6p/Vps39p and Vam2p/Vps41p (Rieder and Emr, 1997; Seals et al., 2000; Wurmser et al., 2000) (reviewed by Bowers and Stevens, 2005).

Vam6p/Vps39p was shown to be required for vacuolar protein sorting in yeast. Yeast Vps39p-null mutants exhibit highly fragmented vacuolar morphogenesis and mutant cells accumulate numerous vesicular structures scattered throughout the cytoplasm (Nakamura et al., 1997). Similarly, overexpression studies in cultured HEK cells have implicated Vam6p in the clustering and fusion of lysosomes and late endosomes (Caplan et al., 2001) and blocking Vam6p function with antibodies suggests a possible role in sperm cells during their interactions with the *zona pellucida* in mice (Brahmaraju et al., 2004).

We have identified a zebrafish mutant (*leberknödel*; *lbk*) that carries a mutation in the zebrafish homologue of Vam6p/Vps39p and displays phenotypes similar to those observed in humans suffering from ARC syndrome, CHS, HPS and GS. Our studies reveal multi-systemic defects in *lbk*, including a hypopigmentation of skin melanocytes and the retinal pigment epithelium (RPE). Moreover, *lbk* displays defects in internal organs (liver, intestine) and the innate

[1]Swiss Federal Institute of Technology, Department of Biology, and Brain Research Institute of the University of Zurich, Winterthurerstrasse 190, CH-8057 Zurich, Switzerland. [2]Institute of Zoology, University of Zurich, Winterthurerstrasse 190, CH-8057 Zurich, Switzerland. [3]Max Planck Institute for Developmental Biology, Spemannstrasse 35, D-72076 Tübingen, Germany.

*Present address: Research Institute of Molecular Pathology (IMP), Dr-Bohr-Gasse 7, A-1030 Vienna, Austria
†These authors contributed equally to this work
‡Author for correspondence (e-mail: stephan.neuhauss@zool.uzh.ch)
§Present address: Center for Brain Research, Medical University of Vienna, Spitalgasse 4, A-1090 Vienna, Austria

Accepted 23 October 2007

immune system. Affected cells display increased numbers and enlarged intracellular vesicles. Physiological and behavioural analyses of visual function in *lbk* uncovered a reduced visual ability. These analyses suggest that Vam6p/Vps39p has essential functions in a range of tissues during zebrafish development. Notably, no animal model to study the function of Vam6p/Vps39p in vivo has been reported to date.

MATERIALS AND METHODS

Fish maintenance and strains

Zebrafish (*Danio rerio*) were kept under standard conditions. Strains used in this study were: Tü (Haffter et al., 1996), WIK (Dahm et al., 2005) and lbk^{t20290}. Staging of embryos in hours (hpf) and days post-fertilization (dpf) was carried out as previously described (Kimmel et al., 1995).

Transplantations

Transplantations were performed as described (Ho and Kane, 1990). Mosaic animals were generated by transplanting 30-40 cells from 3-4 hpf wild-type Tü embryos into the animal pole region, including prospective ectodermal domains, such as the eye and neural crest domains (Kimmel et al., 1995), of age-matched embryos obtained by crossing two $lbk^{+/-}$ carriers. Larvae displaying a clear $lbk^{-/-}$ phenotype were scored for the presence of skin melanocytes and RPE cells displaying wild-type levels of melanin.

Histology, immunohistochemistry and TUNEL assay

For histological analyses by light microscopy (LM), larvae were fixed in 4% paraformaldehyde (PFA) in PBS (pH 7.2) at 4°C overnight and washed three times in PBS. The embryos were dehydrated in a standard ethanol series, infiltrated and embedded in Technovit 7100 (Heraeus Kulzer, Germany) for sectioning. Sections (3 μm) of different developmental stages of mutant and wild-type larvae were cut with a glass knife and mounted on Superfrost Plus slides (Microm International, Switzerland). The sections were subsequently stained with 0.5% Toluidine Blue in a 1% sodium tetraborate buffer (pH 9.2) and analysed using an Axioscope 2Mot (Zeiss, Jena, Germany) connected to an AxioCamHR colour camera using the AxioVision 3.0 software (Zeiss).

For ultrastructural analysis by transmission electron microscopy (TEM), larvae were fixed in 2% PFA and 2.5% glutaraldehyde in 0.1 M HEPES buffer (pH 7.2) at 4°C overnight and subsequently washed three times in HEPES buffer. Larvae were then postfixed with 1% OsO_4 in 100 mM PO_4 buffer (pH 7.2) for 1 hour on ice, washed with double distilled H_20, treated with 1% aqueous uranyl acetate for 1 hour at 4°C, dehydrated through a graded series of ethanol, infiltrated with ethanol/resin mixtures and embedded in Epon (using glycidether 100 from Roth, Karlsruhe). Ultra-thin sections were collected on coated slot grids, stained with uranyl acetate and lead citrate and viewed in a Philips CM 10 electron microscope.

For immunohistochemistry, larvae were fixed in 4% PFA in PBS (pH 7.2) for 45 minutes at room temperature, cryoprotected in 30% sucrose for at least 2 hours, embedded in OCT TissueTek (Jung-Leica; Tissue Freezing Medium) and frozen in liquid nitrogen (N_2). Sections (20 μm) were cut at –20°C, mounted on SuperFrost Plus slides, fixed in ice-cold acetone for 1 minute and stored at –20°C. For further use, slides were thawed, air-dried, washed three times in PBS (0.5×, pH 7.4) and blocked with a solution of 20% normal goat serum and 2% bovine serum albumin in PBS containing 0.3% Triton X-100 (PBST) for 1 hour. Sections were then incubated for 2 hours at 4°C in the primary antibody. Primary antibodies used in this study were anti-glutamine synthetase (1:700; Chemicon, Temecula, USA) and anti-rhodopsine (1:200; MilanAnalytica, LaRoche, Switzerland). Antibodies were diluted in PBST. After three washes in PBST, sections were incubated in Alexa546-coupled anti-mouse secondary antibody (1:500; Molecular Probes/Invitrogen, Eugene, OR) for 1 hour, washed three times in PBST, mounted in glycerol and analysed with an Axioscope fluorescence microscope as described above. Apoptosis was detected using the TUNEL (TdT-mediated dUTP nick-end labelling) method on 35 μm cryosections. TUNEL staining was performed using the Cell Death Kit (Roche Molecular Biochemicals) according to the manufacturer's protocol. Oil red O in dextrin was used to visualise lipid-containing vesicles in cryosections (20 μm). Confocal laser scanning microscopy (CLSM) was performed with an LSM510 (Zeiss) and 25× PlanNeofluar and 63× PlanApochromat oil immersion objectives (Zeiss).

Genetic mapping of *lbk* and radiation hybrid mapping of *vam6*

Map crosses were set up between heterozygous $lbk^{+/-}$ (Tü background) and wild-type WIK zebrafish. The offspring from these crosses were inbred and homozygous $lbk^{-/-}$ and sibling F2 progeny were collected and their DNA extracted. Bulked segregant analysis on 48 $lbk^{-/-}$ larvae and 48 siblings, respectively, was carried out using 192 simple sequence length polymorphisms (SSLP markers) distributed over the entire genome (Geisler, 2002). Further fine mapping was performed using the total DNA of single homozygous mutant larvae. DNA extraction and PCR were performed as described (Geisler, 2002). The zebrafish *vam6* gene was radiation hybrid (RH) mapped on the Goodfellow T51 RH panel as described (Geisler, 2002) using six independent primer pairs (Table 1). PCRs for RH mapping were carried out independently in triplicate.

Cloning of zebrafish *vam6*

A putative zebrafish *vam6* gene was identified via a homology search of the Zv5 Ensemble database (http://www.ensembl.org/Danio_rerio) using the human Vam6p protein sequence as query. Total RNA was isolated from adult zebrafish eyes using the RNAeasy kit (QIAGEN, Switzerland) according to the manufacturer's instructions. cDNA was synthesised using the SuperScript III Reverse Transcriptase Kit (Invitrogen, Switzerland) as described in the manual. The zebrafish *vam6* cds was cloned using primers designed against the start and stop regions of the *vam6* cDNA (Table 2), respectively, using homology with the human *VAM6* gene (*VPS39* – Human Gene Nomenclature Database). To obtain 5′ sequences of the *vam6* cDNA, RACE-PCR was carried out with the SMART RACE cDNA Amplification Kit (Clontech, Switzerland). For RACE primers used to amplify 5′ regions of the *vam6* cDNA, see Table 2. PCR products were cloned into the pCRII-Vector (Clonetech), sequenced with T7 and SP6 primers and submitted to GenBank (Accession Number, EF446162).

Allele screen

Heterozygous $lbk^{+/-}$ carriers were crossed to a collection of ENU-mutated Tü zebrafish and the offspring screened for phenotypes equivalent to that of $lbk^{-/-}$, indicating non-complementation of the novel allele with the *lbk* mutation. Total genomic DNA from 5 dpf larvae showing an *lbk*-like phenotype was extracted, all 24 exons of the *vam6* gene were amplified and the PCR products sequenced (Table 3). All PCR and sequencing reactions were performed independently in triplicate.

Optokinetic response measurements and electroretinogram recordings

Optokinetic response (OKR) measurements were performed as described previously (Rinner et al., 2005b). Briefly, single larvae were placed in the centre of a Petri dish (35 mm diameter) filled with 3% pre-warmed (28°C) methylcellulose facing with their right eye a screen at an apparent distance of

Table 1. Primer pairs used for the radiation hybrid (RH) mapping of the zebrafish *vam6* gene on the Goodfellow T51 RH panel

RH primer pair	Sense primer	Antisense primer
1	ATTTTGTGTCTGCAGGTGTATC	TAGGATTTAGTGGTGGACGCTC
2	TGTCACTGCTGCGCATGTATCT	TGTGGTGAAGCTGAAGGACGTT
3	AGCAGTCTGAATCTGGTGAGG	CACGCATATAGAGTTCTCACACC
4	GGACGTGGCTCAATCAAGG	GGGATGTCAGTCCAGTTGAGG
5	AACTGCGCATGTGTGTTGC	GAGGGCACATTTCTGAGTGC
6	TGCTCTTCCCTCTTGTAGATCC	TCTTGCGGCTCTTGATGG

Table 2. Primer pairs used for the cloning of the zebrafish *vam6* cDNA and detection of zebrafish *vam6* expression in zygotes and 24 hpf embryos

Experiment	Sense primer	Antisense primer
Cloning of *vam6* cds	CAGGAGATTCTACGGTGTTTGG (upstream of START)	AAAGTCAGATCCAGACAGAAAGC (downstream of STOP)
Cloning of *vam6* cds	TGTTTTCGTGTTCTGGTTTTCG (upstream of START)	AAAGTCAGATCCAGACAGAAAGC (downstream of STOP)
5′ RACE PCR	CACGCATATAGAGTTCTCACACCACG	Universal primers as supplied with the SMART RACE cDNA Amplification Kit (Clontech, Switzerland)
Nested 5′ RACE PCR	GAGCAGTGACATCTCCCTGTAATTCG	Universal primers as supplied with the SMART RACE cDNA Amplification Kit
Detection of short *vam6* fragment by PCR	ATGCATGACGCGTACGAACCAGTTC	GGGATGTCAGTCCAGTTGAGG
Detection of long *vam6* fragment by PCR	CAGGAGATTCTACGGTGTTTGG	AAAGTCAGATCCAGACAGAAAGC
Detection of β-actin fragment by PCR	GAGAAGCTGTGCTATGTGG	TTGCCGATGGTGATGACC
Detection of *pmel17* fragment by PCR	TTCATGGAATTCACAGATGTATCC	GAACTGAGTGGATACATAACCAAGG

4.65 cm within their visual field. Moving sine-wave gratings were projected by a HP vp6111 projector onto the screen. The projection size on the screen was 8×6 cm, subtending a visual angle of 65.6° horizontally and 53.1° vertically. Eye movements were recorded by an infrared-sensitive CCD camera triggered by the visual stimulation. A custom developed programme based on the LabView IMAQ software (National Instruments, version 5.1) was used to control the stimulation and the camera as well as to analyse the resulting images. Contrast sensitivity functions for mutant and wild-type larvae were measured by the eye velocity as a function of the contrast of the moving grating. Statistics were derived as described previously (Rinner et al., 2005a) by bootstrap sampling of differences between randomly drawn samples (n=10,000) from a pooled data set of wild-type and mutant larvae. The significance level chosen was at 5% for all experiments.

For recordings of electroretinograms (ERGs) (Makhankov et al., 2004), 5 dpf larvae were dark-adapted for at least 30 minutes prior to positioning them in the recording chamber. The recording chamber was shielded from interference from external sources of electromagnetic radiation by placing it inside a tight Faraday cage. Each larva was placed on its side on the surface of a moist sponge with E3 medium (5 mM NaCl, 0.17 mM KCl, 0.33 mM $CaCl_2$ and 0.33 mM $MgSO_4$) and paralyzed by directly adding a drop of the muscle relaxant Esmeron (0.8 mg/ml; Organon Teknika, Eppelheim, Germany) onto the larva. An Ag/AgCl electrode system was used to record the ERG responses. The recording electrode was positioned on the centre of the cornea. The reference Ag/AgCl pellet was placed under the body of the larva. All pre-recording steps were carried out under dim red light illumination. An additional 5-minute period in complete darkness was chosen to adapt the larva to dark prior to measurements. White light stimuli (100 mseconds) were used to elicit ERG responses with interstimulus intervals of 5 seconds. Light stimuli were fixed at five relatively different light intensities ranging from 2 lux (OD 5) to 20,000 lux (OD 0). Unattenuated light stimulus intensities were measured over the head of the larvae using a light meter (Tektronix J17, Texas Instruments, USA) and found to account for 3100 lux (optical density (OD) equal to 0 log units). Different light intensities were adjusted using neutral density filter wheels. A virtual instrument (VI) under NI LabVIEW 5.1 was developed for use in all experiments. Sampling was carried out in buffered acquisition mode with a sampling rate of 1000 Hz. The resulting ERGs, as the corneal sum field potentials of the retina in response to light, are shaped like in other vertebrates: a small negative deflection, termed the a-wave, which reflects photoreceptor activation, is followed by a stronger positive deflection, the b-wave, which reflects second order neuron activation. The small a-wave is often masked by the much larger b-wave because of interference. Therefore, in contrast to the b-wave, the a-wave is not a robust measure in larval zebrafish. As a consequence, the b-wave was taken as an indirect measure of outer retina activation. For rescue experiments, a light intensity of 6000 lux was chosen to elicit ERG responses in sibling and $lbk^{-/-}$ larvae. ERG responses obtained from one larva were averaged three to seven times depending on signal-to-noise ratio. Statistical analysis was performed using GraphPad Prism4 (GraphPad Software, San Diego, CA) software and graphs were generated using Origin v.7 (OriginLab, Northampton, MA).

Bacteria injections

Salmonella enterica serovar Typhimurium expressing DsRed (van der Sar et al., 2003) were injected with a FemtoJet injection apparatus (Eppendorf) at a constant pressure of 80 hPa for 0.5 seconds into the common cardinal vein of 48 hpf larvae embedded in low-melting point agarose as previously described (van der Sar et al., 2003). To ensure delivery of equal amounts of bacteria, mutant and sibling larvae were injected with the same injection capillary and the injection of the bacteria was monitored under a fluorescence stereo-microscope (Zeiss). For bacterial counts, larvae were macerated in PBS and plated onto ampicillin-containing bacterial plates as described (van der Sar et al., 2003; van der Sar et al., 2006). Bacterial growth was assessed after 24 hours of incubation at 37°C with a fluorescence stereo-microscope.

Rescue experiments

The rescue was performed by injecting a pSGH2 vector containing the *vam6* cds under the control of a heat-shock promoter (Bajoghli et al., 2004) into one-cell stage embryos derived from a cross of two $lbk^{+/-}$ individuals. At 3 dpf, injected larvae were heat shocked at 38°C for 2 hours and subsequently transferred back to 28°C. The extent of the rescue was determined at 5 dpf by assessing the level of pigmentation in skin melanocytes and RPE and in ERG measurements.

Morpholino knock-down

A 25 nucleotide morpholino antisense oligonucleotide was designed against the ATG region of the *vam6* mRNA: GAACTGGTTCGTATGCGTCG-TGCAT. The morpholino was injected using a pressure of 30 hPa for 4 mseconds into one-cell stage wild-type embryos at different oligonucleotide concentrations: 100 μM, 500 μM and 700 μM, corresponding to approximately 1.5 ng, 7.5 ng and 10.5 ng of morpholino. As a control, the generic control morpholino provided by GeneTools (Philomath, OR) was used.

Detection of *vam6* expression

For PCR analysis, total RNA was isolated from 100 wild-type zygotes and 24 hpf embryos, respectively, using the RNAeasy kit and cDNA synthesised using the SuperScriptIII Reverse Transcriptase kit. PCR was performed at an annealing temperature of 60°C for 35 cycles using primers listed in Table 2.

Whole-mount in situ hybridisation

Sense and antisense probes for in situ hybridisation were in vitro transcribed from a linearized pCRII-Vector containing the full-length *vam6* cds using SP6 and T7 polymerases, respectively, in the presence of digoxigenin-coupled nucleotides (DigRNA labelling kit; Roche Molecular Biochemicals, Switzerland). Transcripts were hydrolysed to obtain fragments of ~300-500 nucleotides in length. To prevent melanisation of skin melanocytes and the

Table 3. Primer pairs used to amplify and sequence the 24 exons of the *vam6* gene from total genomic DNA of 5 dpf larvae showing an *lbk*-like phenotype (*lbk) in the allele screen**

Exon	Sense primer	Antisense primer
Exon 1	TGGGTGTTTTCGTGTTCTGG	CAAATGAAGTGAAGAAAAGATGAGC
Exons 2 to 5	TGACCTGACCATTTAAATCAGACC	TGTGGCAACTGTGATTTTGC
Exons 6 and 7	ACTTTTCTGTCAATGTCTTCTGTCC	CAAGCTGGTATCAACACTAATGAGG
Exon 8	CGTGCTACCAAGCAAAAAGG	CTCAGGACGGGGAAAAGG
Exon 9	TGCAAACCTGTTTGATCACG	TTACAGACTCCTCCTGCTCACC
Exons 10 and 11	AAAAAGTGGTTGCAGCTTCC	CAAACCCGTCATTCTGTGC
Exons 12 and 13	TCTGATGTGTAAAAGCTGATGTGC	TTTGCACAAAGCAGAAAGAGC
Exon 14	TGTCACATGTTGTTAGGAAAAGG	AAAAGCATTTCATAGCCAGAAGG
Exon 15	TGACTCCAGACCTGTGAAACG	AAGAAAATTGCACGGTAAATCG
Exons 16 and 17	CGAAGTCTACATGTCGTGAACC	ATCATCCAGCCTGTTTGTGG
Exons 18 and 19	GGAGAGCTTTCCATCTTCACG	AAGACTGCCAGACACTAAAGACG
Exon 20	ACAAGCTGCCGACATGTATAGC	GAATGTTGCATCATACAGAACAGG
Exon 21	GGTGACACATTTTCTGTGAACG	CGTTCTCACTTTATCCAGAATCG
Exon 22	TTTTGCAGGCAGATTAAGTTCC	CAATTGCACAGAAAACCAAACC
Exon 23	AAGAGTGACAAGGCATAATTACAGG	TTTTTAACGGTGACGGTTGG
Exon 24	GGATGTGTGTAAGCAGTTTGAGG	CATCTTAAGTGAAGCCGAGTGG

In cases where a primer pair was used to sequence more than one exon, intervening introns were also amplified and sequenced.

RPE, embryos used for in situ hybridisation were treated with 0.2 mM PTU (1-phenyl-2-thiourea; Sigma). PTU-treated embryos were staged, fixed in 4% PFA in PBS (pH 7.25) at 4°C overnight, dehydrated in a standard methanol series and stored in 100% methanol at –20°C. In situ hybridisation was performed using an automated in situ hybridisation apparatus (Hölle&Hüttner, Tübingen, Germany). Hybridisation was carried out overnight at 58°C. Probe detection was performed with an alkaline phosphatase-coupled anti-Dig Fab-fragment (Roche) and NBT/BCIP staining buffer. Stained embryos were cleared with 50% methanol/50% glycerol and transferred into 100% glycerol for imaging.

RESULTS

lbk mutants show hypopigmentation and hepatomegaly

The zebrafish mutant *leberknödel* (*lbk*^{t20290}) was identified in a large-scale ENU mutagenesis screen (Glass and Dahm, 2004). External analyses revealed that, starting at 3 dpf, *lbk*$^{-/-}$ larvae show a pronounced hypopigmentation of skin melanocytes and the RPE. Instead of the evenly black melanocytes characteristic of wild-type larvae, *lbk* melanocytes show only scarce and patchy pigmentation (Fig. 1, see Fig. S1 in the supplementary material). It is interesting that in addition to melanosome-containing cells the iridophores are affected in *lbk*. Iridophores derive their reflective properties from vesicular organelles containing guanine crystals (Morrison and Frost-Mason, 1991). These light reflections are absent in *lbk*, both in the eye and body, at all stages of development (Fig. 1E-H), indicating that the biogenesis of these organelles is disrupted. We cannot, however, exclude the possibility that iridophores are missing altogether, although, in view of the overall *lbk* phenotype, this possibility appears unlikely. Further to the pigment cell phenotypes, starting at 4 dpf, the intestinal tract of *lbk* develops a brownish discolouration (Fig. 1A-F,I,J) and the liver becomes enlarged (Fig. 1I,J). *lbk*$^{-/-}$ larvae fail to develop swim bladders and die between 7 and 8 dpf.

Mapping and candidate gene approach identify a mutation in the *vam6* gene as underlying the *lbk* phenotype

To identify the mutation underlying the *lbk* phenotype, we mapped the mutation on the zebrafish genome. Pooled DNA of 48 *lbk*$^{-/-}$ and 48 sibling 5 dpf larvae, respectively, was tested with 192 SSLP markers (Knapik et al., 1998) resulting in a linkage of the mutation to chromosome 17 between markers z22083 and z4053 (Fig. 1K). To narrow down the critical interval of the mutated locus, we tested additional SSLP markers located in this genomic region. Analysis of 282 meioses identified z9692 and z4053 as the closest SSLP markers (Fig. 1K).

As the phenotype observed in *lbk* suggests a defect in endosomal vesicle trafficking (see below), we performed RH mapping of several genes involved in this process. This approach resulted in a linkage of the zebrafish *vam6* gene to the EST fc27c07.x1 on chromosome 17. This EST is located in close proximity to z9692 on the T51 RH map (Fig. 1K) (Geisler et al., 1999). Given this close linkage, we cloned and sequenced the zebrafish *vam6*-coding sequence (cds), which has a length of 2628 bp corresponding to a protein of 875 amino acids (see Fig. S2 in the supplementary material).

Sequencing of pooled *vam6* cDNA from *lbk*$^{-/-}$ larvae and phenotypically wild-type siblings, respectively, revealed a nonsense mutation at position 1066 of the *vam6* cds (Fig. 1L), which segregated with the mutant phenotype. This point mutation was confirmed by sequencing exon 11 from genomic DNA of the larvae identified as recombinant in the fine mapping approach. All 15 individuals displaying the *lbk* phenotype were genotypically homozygous for the point mutation, whereas all phenotypically wild-type individuals were either heterozygous or homozygous for the wild-type allele (not shown). The putative truncated protein product lacks the C-terminal 520 amino acids, including the central clathrin homology (CLH) repeat domain, which has been demonstrated to play an essential role in the clustering and fusion of lysosomes (Caplan et al., 2001), and Ypt7p-interacting sequences (Wurmser et al., 2000) (Fig. 1M,N).

To identify additional *lbk* alleles and thus confirm that a mutation in *vam6* underlies the *lbk* phenotype, we performed complementation analyses with described mutants displaying similar external phenotypes (Glass and Dahm, 2004; Kelsh et al., 1996). These analyses identified no additional *lbk* alleles. We therefore performed an allele screen by crossing heterozygous *lbk*$^{+/-}$ individuals with ENU-mutated Tü zebrafish. Over 1000 genomes were screened for external phenotypes equivalent to that observed in *lbk*, indicating non-complementation of the novel allele with the *lbk* mutation. This approach identified a compound heterozygous larva (*lbk**; see Fig. S3 in the supplementary material) harbouring in one allele of the *vam6* gene the original C→T exchange found in *lbk* and in the second allele a T→A exchange at position 374 of the *vam6* cds (Fig. 1O). The latter mutation results in the exchange of a

conserved methionine residue for a lysine at amino acid position 125 in the N-terminal citron homology (CNH) domain of the Vam6p protein (see Figs S2, S3 in the supplementary material). This domain has been shown to be required for lysosome clustering and fusion (Caplan et al., 2001). Importantly, siblings from the same cross carrying the *lbk* nonsense allele, did not carry the T→A exchange identified in *lbk** compound heterozygotes (Fig. 1O), confirming that this mutation disrupts Vam6p in the *lbk** larva. Sequencing of 142 *vam6* alleles confirmed that this T→A exchange does not occur in the genetic pool from which the founder fish for the ENU-mutagenesis were derived (see Fig. S3 in the supplementary material). The compound heterozygous mutant was not viable and the allele was not recovered to generate a permanent line. Therefore, the information that can be derived from the analysis of the *lbk** mutant is limited to the one experiment reported here.

The *lbk* mutation acts cell autonomously

To investigate if the defect caused by the mutation in *lbk* is cell-autonomous, we performed blastomere transplantations. Wild-type cells from 1000-cell stage embryos were transplanted into age-matched embryos obtained from a cross of two heterozygous *lbk* carriers. At 5 dpf, the resulting larvae were screened and larvae with a predominantly $lbk^{-/-}$ mutant skin phenotype (as judged by the presence of strongly hypopigmented melanocytes) were investigated for the presence of melanocytes of wild-type appearance. As the $lbk^{-/-}$ phenotype is fully penetrant such that mutants never display melanocytes with normal levels of pigmentation, melanocytes of wild-type appearance had to be derived from transplanted cells. In four independent experiments, a total of 26 $lbk^{-/-}$ background larvae displaying melanocytes with wild-type pigmentation in their skin were identified (see Fig. S4 in

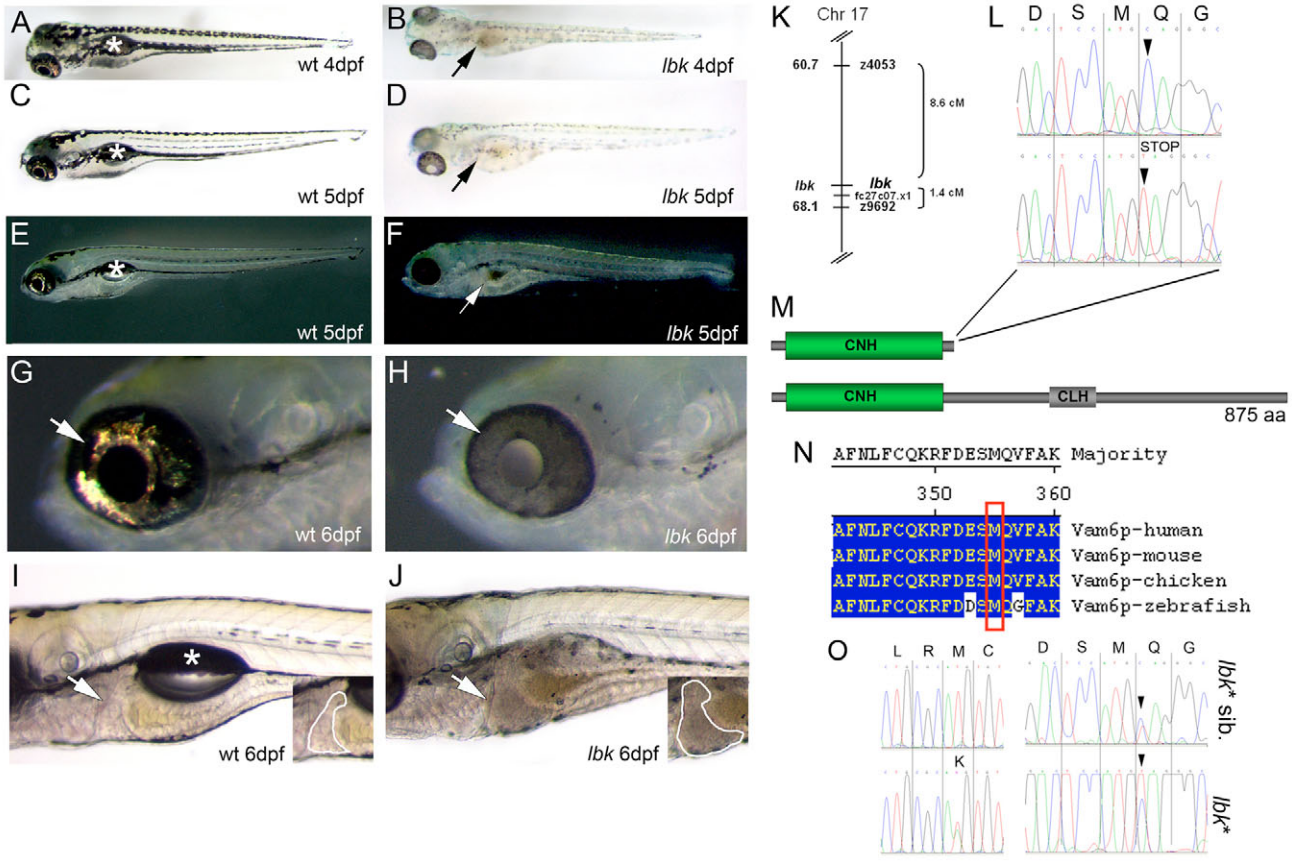

Fig. 1. A mutation in *vam6* causes hypopigmentation and hepatomegaly in *lbk*. (**A-D**) Bright-field images show the hypopigmentation of skin melanocytes and the RPE, and a brownish discolouration of the intestinal tract (B,D, arrows) in *lbk*. Asterisks in A,C indicate the swim bladders in wild-type larva. (**E-H**) Dark-field images show an absence of iridophore reflections in the *lbk* skin and eye (G,H; arrows). Note the translucency of the *lbk* RPE in H. Arrow in F indicates the intestinal tract. Asterisk in E indicates the lac of swim bladder. (**I**,**J**) *lbk* larvae display an enlarged liver (insets in I,J; outlined areas) and lack swim bladders (asterisk). (K-O) The gene for Vam6p is mutated in *lbk*. (**K**) Genetic mapping of *lbk* resulted in linkage to SSLP markers z9692 and z4053 on chromosome 17. RH mapping of zebrafish *vam6* resulted in linkage to EST fc27c07.x1, which was found to be located close to z9692 on the T51 RH map and thus served as an anchor to link the two maps. (**L**) Sequencing of cDNA from $lbk^{-/-}$ and homozygous wild-type larvae revealed a nucleotide exchange at position 1066 from C→T (arrowheads), resulting in a premature STOP codon. (**M**) Domain structures of the wild-type Vam6p (bottom) and the protein truncated in *lbk* lacking the C-terminal 520 amino acids (top), including the clathrin homology (CLH) repeat domain and Ypt7p-interacting sequences. (**N**) Sequence alignment of human, mouse, chicken and zebrafish Vam6p proteins shows the high level of conservation in the region affected by the mutation (red box). (**O**) Sequencing of the complete *vam6* cds from the *lbk** mutant revealed that this larva was heterozygous at two positions: the C→T nucleotide exchange identified in *lbk* (right panel, lower trace; arrowhead) and a novel T→A exchange at position 374 of the *vam6* cds (left panel, lower trace). The latter results in the exchange of a conserved methionine (M) at amino acid position 125 for a lysine (K) in the N-terminal citron homology (CNH) domain (see Figs S2, S3 in the supplementary material). Sequencing of the complete *vam6* cds from *lbk** siblings showed the heterozygous presence of the *lbk* mutation (right panel, upper trace; arrowhead), but the absence of the T→A exchange at position 374 (left panel, upper trace).

the supplementary material). The development of transplanted wild-type cells into normally pigmented melanocytes in an *lbk*$^{-/-}$ background indicates that the *lbk* mutation acts cell autonomously.

lbk larvae have a compromised RPE and are severely visually impaired

Hypopigmented retinas often have additional defects and affected zebrafish were shown to display decreased visual ability (Schonthaler et al., 2005). Similarly, in humans several pathological conditions with RPE hypopigmentation are associated with more generalised ocular symptoms. This prompted us to examine the eye phenotype in *lbk* more closely. Histological analyses revealed that the overall patterning of the neural retina is normal (Fig. 2A-F). However, sections taken at different developmental stages revealed not only a severe hypopigmentation of the RPE, but also a progressive thickening (Fig. 2A-H) up to three times the thickness of the wild-type RPE (Fig. 2R). This thickening results from an increase of RPE cell size, rather than increased numbers of RPE cells (Fig. 2S). TEM analyses of *lbk* revealed substantially fewer and mostly immature and aberrantly shaped melanosomes (Fig. 2I-N,Q). As melanin is, however, present in the *lbk*$^{-/-}$ RPE and skin melanocytes (see Fig. S5 in the supplementary material), the mutation affects the biogenesis of melanosomes rather than melanin biosynthesis. This is supported by the observation that the number of mature melanosomes is substantially reduced in *lbk* (Fig. 2V).

In addition to optically shielding photoreceptor cells (PRCs), the RPE is essential for PRC function by phagocytosing shed PRC outer segments. Outer segments harbour the photopigments that allow the detection of light and the shedding of parts of these segments is an essential process in the maintenance of normal PRC function. The RPE cytoplasm in *lbk* is filled with numerous vesicles whose number increases between 5 and 7 dpf (Fig. 2I-L). Some of these vesicles contain thick membrane stacks reminiscent of the membrane discs in PRC outer segments (Fig. 2M,N), suggesting a defect in the fusion of endocytic vesicles with lysosomes.

To test this hypothesis, we used rhodopsin as a molecular marker for rod outer segments (Fig. 2O,P). *lbk* larvae (5 dpf) show an increase in rhodopsin-positive vesicles inside the RPE, while in the wild-type, rhodopsin antibodies only label continuous rod outer segments. Quantification confirmed that the *lbk* RPE contains increased numbers of outer segment-containing vesicles (Fig. 2T). Staining of eye cryosections with Oil Red O confirmed the presence of numerous lipid-containing vesicles in the *lbk* RPE (Fig. 4J). These data further suggest a failure in the mutant RPE to metabolise phagocytosed PRC membrane stacks.

At 5 dpf, the PRC outer segments are fully developed in the zebrafish. In *lbk* mutants, however, they are reduced in length and their regular palisade arrangement is disrupted (Fig. 2I-L,U). Moreover, the microvilli from the RPE that normally interdigitate with the outer segments, cannot be detected. As development proceeds, these phenotypes get stronger resulting in PRCs with very short or even no outer segments (Fig. 2L).

Although we found the outer retina to be severely affected, the inner retina showed no evidence of morphological alterations in *lbk* (Fig. 2A-F). Similarly, staining of retinal Müller glia cells, which span the entire inner retina and are thus a good marker for inner retinal architecture, revealed no differences in their number, arrangement and morphology between wild-type and *lbk*$^{-/-}$ larvae (see Fig. S6 in the supplementary material). Starting at 7dpf, however, apoptotic cells can be detected in the neural retina (Fig. 2W).

To analyse the physiological effect of the *lbk* mutation on visual performance, we tested larvae by optokinetic response (OKR) measurements. In this test, eye tracking movements of immobilised larvae exposed to moving visual stimuli are used to assess visual ability. In contrast to wild-type larvae, moving gratings consistently failed to evoke eye movements in all *lbk*$^{-/-}$ larvae tested, indicating that mutants are behaviourally blind (Fig. 3A). However, this effect is not due to the inability of the mutants to move their eyes, as spontaneous eye movements were regularly observed. We further performed electroretinogram (ERG) analyses of 5 dpf wild-type and *lbk* larvae (Fig. 3B). In wild-type larvae the b-wave amplitude increased with increasing light intensities. In *lbk*, however, it remained small even at high light intensities. At 7dpf, the ERG of *lbk*$^{-/-}$ is flat, indicating that at this stage the mutant retina no longer responds to light stimuli (not shown).

lbk larvae display vesicle phenotypes in the liver and intestinal tract

Subsequent analyses revealed additional phenotypes in internal organs, including the liver and intestine. Starting at 6dpf, the liver of *lbk* larvae becomes progressively enlarged and darkly discoloured (Fig. 1I,J). Histological analyses confirmed this enlargement and showed a significant swelling of liver cells (Fig. 4A,B). This phenotype was confirmed when *lbk*$^{-/-}$ mutants were crossed to a transgenic line, Tg (ef1:GFP), that expresses GFP under the control of the intestinal promoter ef1 (Field et al., 2003) and sections imaged by confocal microscopy (Fig. 4C). To quantify the increase in liver size observed in *lbk*, we related the total liver area to the number of hepatocyte nuclei in a given section. By this measure, 5 dpf *lbk* larvae show a 30% increase of liver cell area compared to their siblings (Fig. 4D).

TEM analyses revealed that the cytoplasm of hepatocytes in *lbk* is filled with numerous, sometimes very large vesicles (up to 30 μm in diameter; Fig. 4E,F), indicative of a defect in vesicle trafficking in this cell type. At 7 dpf, the hepatocytes of *lbk* larvae show substantial necrotic changes (Fig. 4G,H). These changes might also explain the discoloration of the liver observable in external views (Fig. 1J). Oil Red O staining further showed an accumulation of vesicles containing large amounts of lipids in the *lbk* liver (Fig. 4I).

We further examined the intestines of *lbk* and age-matched sibling larvae. TEM analyses of 7 dpf larvae revealed a vesicle phenotype also in the cells of the mutant intestinal bulb. Although wild-type cells contain few large vesicles, the number of vesicles is significantly increased in *lbk* with a concomitant reduction in vesicle size (Fig. 4K,L; see Fig. S7 in the supplementary material). This further indicates a possible defect in the fusion of intracellular vesicles in *lbk*.

The innate immune system is compromised in *lbk* mutants

Similar to RPE cells, macrophages are highly phagocytotically active and contain numerous lysosomes and lysosome-related organelles, such as major histocompatibility complex class II compartments (Raposo and Marks, 2002). This prompted us to examine the morphology of vesicles in this cell type by incubating 7 dpf *lbk* and sibling larvae in Neutral Red, which is selectively retained in macrophage lysosomes (Herbomel et al., 2001). This staining suggests that intracellular vesicles in *lbk* macrophages may be enlarged, seem to display an amorphous shape and are more heterogeneous in size than in wild-type larvae (Fig. 5A,B; inserts).

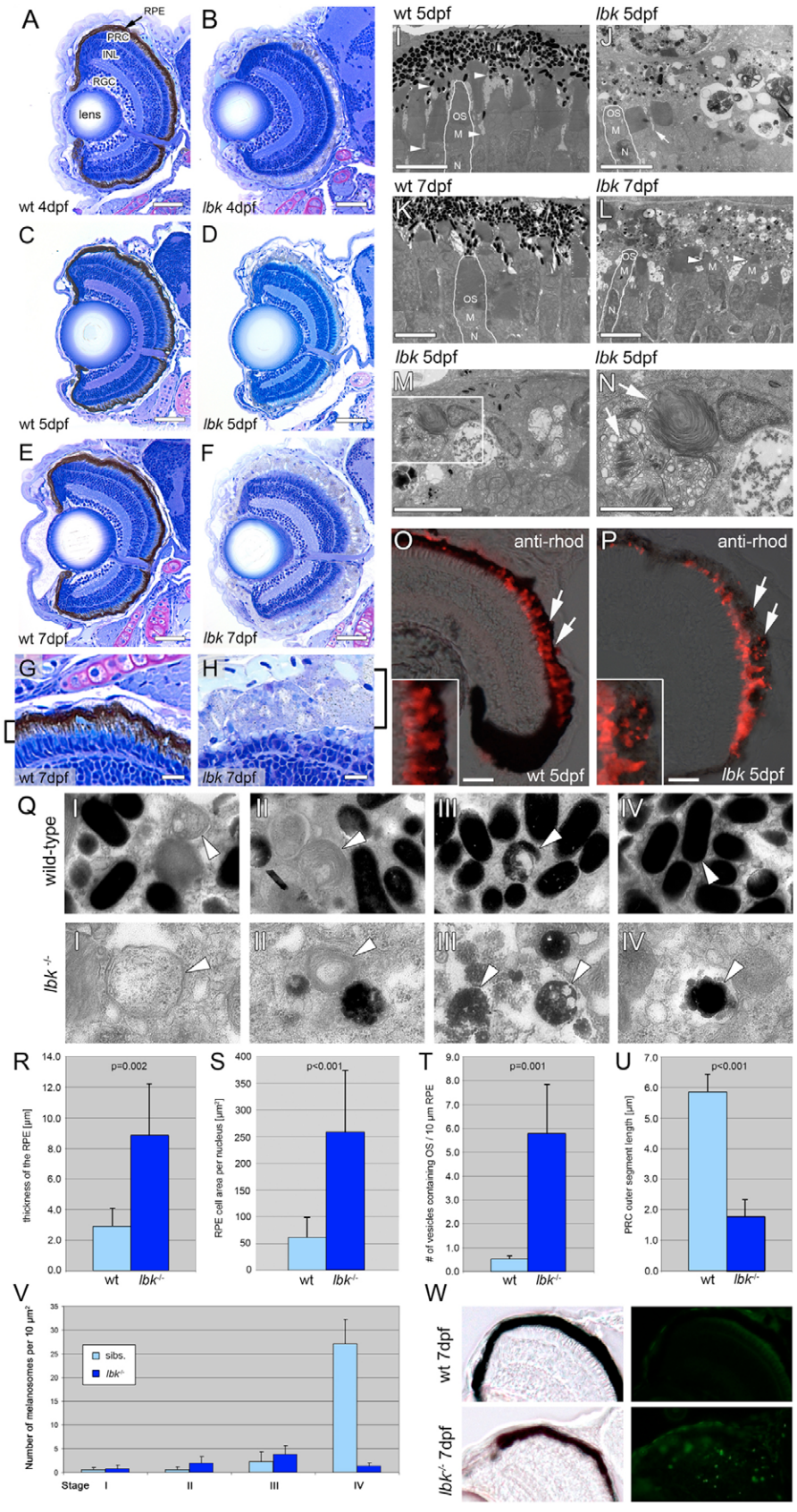

Fig. 2. *lbk* larvae display a severely compromised RPE and shorter PRC outer segments. (**A-H**) Sections of *lbk* (B,D,F,H) and sibling (A,C,E,G) eyes show that overall eye development proceeds normally in *lbk*, including the formation of a multi-layered neural retina. Beginning at 4 dpf (A,D), however, the retinal pigment epithelium (RPE) is severely hypopigmented and becomes progressively inflated. At 7 dpf (E-H), the RPE in *lbk* is threefold thicker than in age-matched siblings (G,H; brackets). The inner retina in *lbk* is morphologically indistinguishable from wild-type siblings. INL, inner nuclear layer; PRC, photoreceptor cells; RGC, retinal ganglion cells. (**I-N**) TEM sections reveal that the *lbk* RPE contains very few mature melanosomes. The majority of melanosomes are aberrantly shaped and show regions that lack pigment. Moreover, the mutant RPE is filled with numerous vesicles. The number of vesicles increases from 5-7 dpf (compare J with L). The microvilli of the RPE (I, arrowheads) that normally interdigitate with the outer segments of PRCs are significantly reduced in *lbk* (J; arrow). Furthermore, the outer segment length is reduced. Some *lbk* PRCs virtually lack outer segments (L, arrowheads). (M,N) Higher magnification of vesicles containing undigested PRC outer segments (arrows) in the *lbk* RPE (N shows a higher magnification of the boxed area in M). M, PRC mitochondria; N, PRC nucleus; OS, PRC outer segment. (**O**,**P**) Merged phase contrast and fluorescence images of eye sections stained for rhodopsin (red) show an increase of discrete rhodopsin-positive vesicles in the *lbk* RPE (P, arrows) versus continuous PRC OS in the wild type (O, arrows). Insets show higher magnifications of parts of the RPE from the sibling and mutant retinas shown in O and P. (**Q**) Images showing melanosomes at different stages of maturation (I-IV) in the sibling (top) and *lbk* (bottom) RPE at 5 dpf. Arrowheads indicate melanosomes of the respective stages. (**R-U**) Statistical analyses of RPE thickness (R), average RPE cell area per nucleus (S), average number of vesicles containing PRC outer segments (T) and PRC outer segment length (U) in sibling and *lbk* larvae at 5 dpf. Error bars indicate standard deviations; *P* values were calculated using Student's *t*-test. (**V**) Quantification of melanosomes at different stages of maturation in the *lbk* and sibling RPE at 5 dpf. Counts represent the numbers of melanosomes in areas of 10 μm^2. Although there are no substantial differences between the numbers of stage I-III melanosomes, mutant larvae contain significantly fewer mature (stage IV) melanosomes. (**W**) TUNEL labelling of cryosections shows increased levels of apoptosis in *lbk* (bottom right). The relatively dark appearance of the mutant RPE results from the thickness of these sections (40 µm). All images were derived from mid-transversal sections of the eye. Scale bars: 50 µm in A-F; 10 µm in G,H; 5 µm in I-M; 2.5 µm in N; 25 µm in O,P.

To obtain functional information on the innate immune system in *lbk*, we injected DsRed-expressing bacteria into mutant and sibling larvae at 48 hpf (Fig. 5C). Phagocytosis of the injected bacteria was complete within 10 minutes of the injection. Clearance of the fluorescent bacteria was monitored by in vivo fluorescence microscopy as well as by plating dissociated larvae onto selective media plates and counting of the resulting bacterial colonies. We found that while siblings efficiently cleared injected bacteria within 32 hours, mutants still contained numerous bacteria (Fig. 5D-M). Importantly, although phagocytosis appeared unaffected in *lbk*, the subsequent failure of the mutant phagocytes to degrade the bacteria indicates a defect in the fusion of phagosomes with lysosomes.

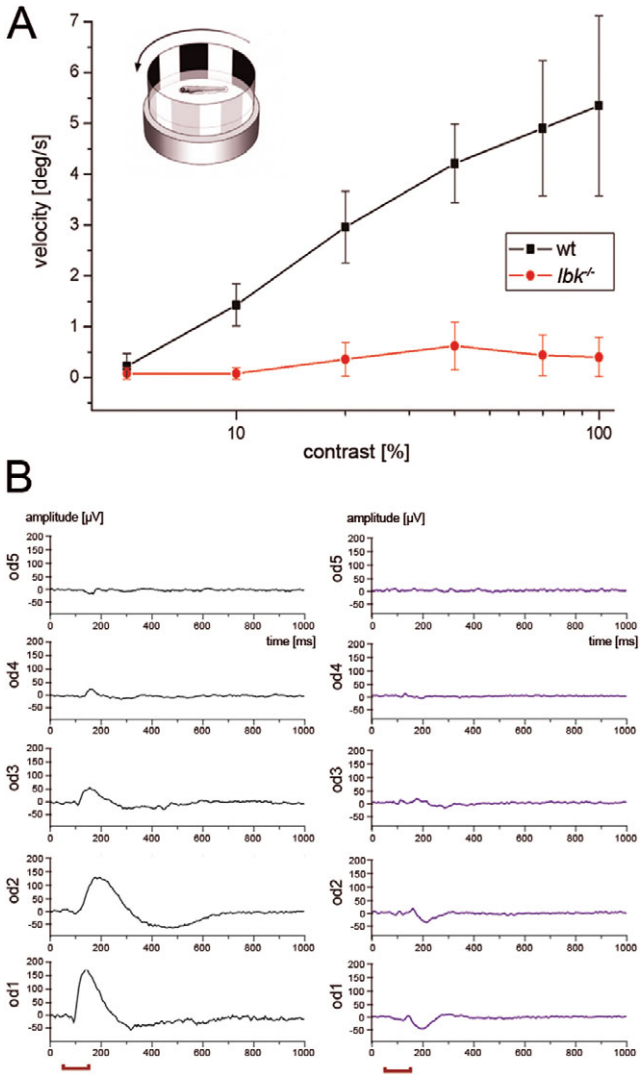

Fig. 3. *lbk* larvae show a strong visual impairment. (**A**) Optokinetic responses (OKRs) of 5dpf *lbk* and sibling larvae (*n*=6) stimulated with a sinusoidal grating. Although sibling larvae show a strong increase in eye tracking velocity with increasing contrast of the moving pattern, *lbk* mutants lack an OKR at all contrast levels, suggesting that the mutants are behaviourally blind. Error bars indicate standard deviations. The difference between wild-type and *lbk* larvae was significant at all levels of contrast. Significance was tested by inference statistics described by Rinner et al. (Rinner et al., 2005a) with a significance level of 5%. (**B**) Electroretinograms (ERGs) of 5 dpf *lbk* and sibling larvae measured over five log intensities of light. Mutant larvae (right) show a dramatically reduced b-wave compared with age-matched siblings (left). Red brackets indicate 100 ms light stimuli.

Rescue and morpholino phenocopy of the *lbk* phenotype

To confirm that a mutation in *vam6* underlies the *lbk* phenotype, we performed a rescue experiment. The zebrafish *vam6* cds was cloned into an expression vector under the control of a heatshock-inducible promoter (Bajoghli et al., 2004). This vector was injected at the one-cell stage and expression induced by heat shock at 3 dpf. In total, three independent experiments were performed and evaluated. To assess the rescue of the mutant phenotype, the larvae were screened at 5 dpf for their external morphology. *vam6*-injected *lbk* larvae developed darker skin melanocytes and RPE (Fig. 6A-C; insets) than uninjected and control vector-injected (no *vam6* cds) *lbk* larvae. The larvae were further tested by ERG analysis to assess the rescue of the visual ability. *vam6*-injected *lbk* larvae showed an increase in the b-wave amplitude to 20-60% of wild-type levels (Fig. 6A-D). By contrast, uninjected control *lbk* larvae did not show a b-wave (Fig. 3B).

To provide further evidence that a mutation in *vam6* underlies the *lbk* phenotype, we designed an antisense morpholino against a region containing the start codon (ATG) of the *vam6* mRNA. Injection of the ATG-morpholino into wild-type embryos at the one-cell stage resulted in a similar, but stronger phenotype than that observed in *lbk* (Fig. 6E). Injection of a control morpholino did not result in larvae displaying any phenotypes (Fig. 6E). The weaker phenotype of *lbk* larvae compared with the *vam6* knock-down could be explained by the presence of maternally supplied wild-type *vam6* mRNA, which could serve as a template for the synthesis of functional Vam6p during early embryonic development. To test this hypothesis, we isolated mRNA from wild-type zygotes, reverse transcribed it into cDNA and performed a PCR analysis. This showed that *vam6* mRNA is maternally supplied in zebrafish (Fig. 6F) and its expression persists through later stages of development (Fig. 6F,G; see Fig. S8 in the supplementary material). The Vam6p protein is part of the HOPS complex, a large multi-subunit protein complex. In this context it is interesting that the mRNA for Vps18, another member of the HOPS complex, has been found to be maternally supplied in zebrafish zygotes in a microarray experiment (http://zf-espresso.tuebingen.mpg.de/).

DISCUSSION

In this study, we provide the first phenotypic description of a lack of *vam6* gene function in a multicellular organism. Zebrafish *lbk* mutants display defects in several tissues and cell types (liver, intestinal tract, macrophages, PRCs, RPE and skin melanocytes) as well as compromised vision and innate immunity. The range of phenotypes resembles pathological symptoms observed in individuals suffering from syndromes caused by defects in lysosomes and lysosome-related organelles (Stinchcombe et al., 2004), including the ARC syndrome, CHS, GS and HPS. For example, CHS, GS and HPS are characterised by a hypopigmentation of the skin and RPE, as well as a significant visual impairment (Barak and Nir, 1987; Clark and Griffiths, 2003; Griscelli et al., 1978; Hermansky et al., 1975). These symptoms are also observed in *lbk* mutants.

Melanosomes are part of the large group of lysosome-related organelles and serve to synthesize and store melanin. The melanocytes in *lbk* mutants display significantly fewer and lighter melanosomes than are observed in wild-type animals. The presence of melanosomes with wild-type levels of melanin pigmentation in

the *lbk* skin and RPE shows that the mutation does not cause a block in melanin synthesis or melanosome biogenesis per se. The increase in immature melanosomes and the substantially decreased number of mature (stage IV) melanosomes in *lbk* rather suggests a significantly reduced efficiency of melanosome maturation, a process critically dependent on the fusion of endosomal vesicles with premelanosomes (Dell'Angelica, 2003). Alternatively, the stop codon mutation we identified in *lbk*, UAG, has been suggested to have intermediate read-through fidelity. Thus, the mutant embryos might retain a low level of functional protein, as has been observed in the human syndromes described in this manuscript and other lysosomal storage disorders (Brooks et al., 2006).

The hypopigmentation of the *lbk* RPE probably contributes to the reduced visual ability. Moreover, the RPE contains numerous vesicles containing undigested PRC outer segments. Although indicating that phagocytosis by the RPE is not compromised, this novel phenotype suggests a defect in lysosome-mediated degradation of phagocytosed outer segments, a central function of the RPE, which may lead to a generalised metabolic dysregulation. As the RPE is essential for maintaining the PRCs, compromising the viability of the RPE will probably also negatively affect PRC function. This notion is supported by our TEM studies, which reveal shortened PRC outer segments. The presence of an a-wave in ERGs, however, suggests that *lbk* PRCs retain at least some functionality

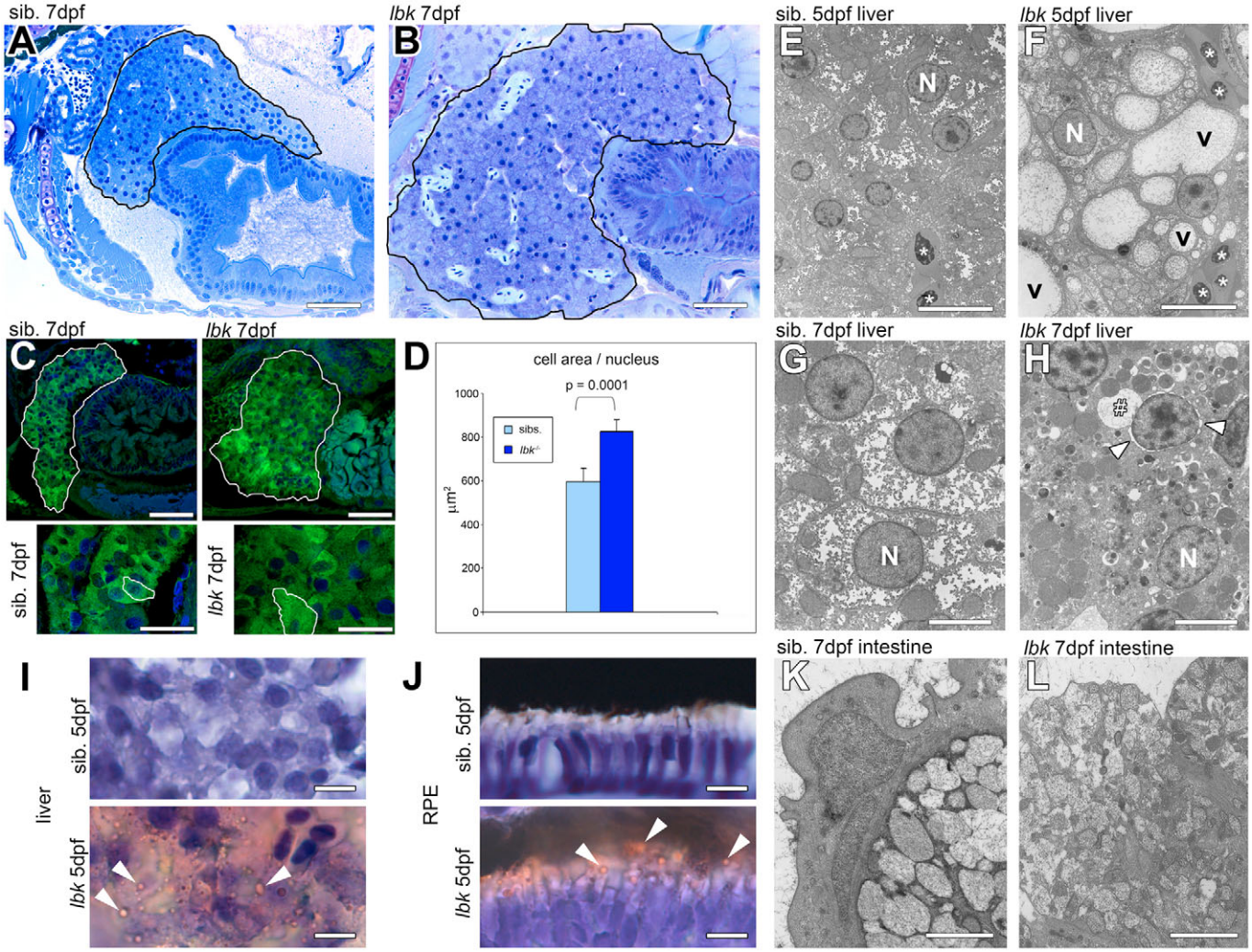

Fig. 4. *lbk* larvae display vesicular phenotypes in liver and intestinal cells. (**A**,**B**) Longitudinal sections showing the liver and part of the intestine. There is a substantial increase in liver size (outlined) in *lbk*. Sections were derived from the same region of the body and images are reproduced at the same magnification. (**C**) Confocal LSM images of larvae expressing GFP under the intestinal promoter ef1 reveal an increase in liver size (top row, outlined) in *lbk*. Nuclei are stained with DAPI (blue). Bottom row shows higher magnifications of regions from livers shown in the top row. Individual liver cells are outlined showing the increase in hepatocyte size in *lbk*. The arrangement of hepatocytes in *lbk* is disorganised. (**D**) Quantification of the average cell area per nucleus in histological sections of livers revealed that the *lbk* liver shows on average an area 30% larger than that of age-matched siblings [n=5 (sibs.), n=7 (*lbk*); P=0.0001]. (**E-H**) Transverse TEM sections of livers show that *lbk* hepatocytes contain numerous large vesicles (v). Asterisks indicate erythrocytes. At 7 dpf, *lbk* hepatocytes display necrotic changes: e.g. a condensation of nuclear chromatin; an increase in the space between the nuclear membranes (arrowheads); a massively inflated ER lumen (#), which is continuous with the nuclear membranes; and numerous vesicles often displaying an electron-dense lumen. N, nucleus. (**I**,**J**) Oil Red O staining of the liver (I) and RPE (J) reveals lipid-containing vesicles (arrowheads) in hepatocytes and the RPE in *lbk*. (**K**,**L**) Transverse TEM sections of the anterior intestine show an increase in number and decrease in size of vesicles in the cells lining the intestine in *lbk*. Scale bars: 50 µm in A,B; 50 µm in C; 25 µm in insets; 10 µm in E,F,I,J; 5 µm in G,H; 2 µm in K,L.

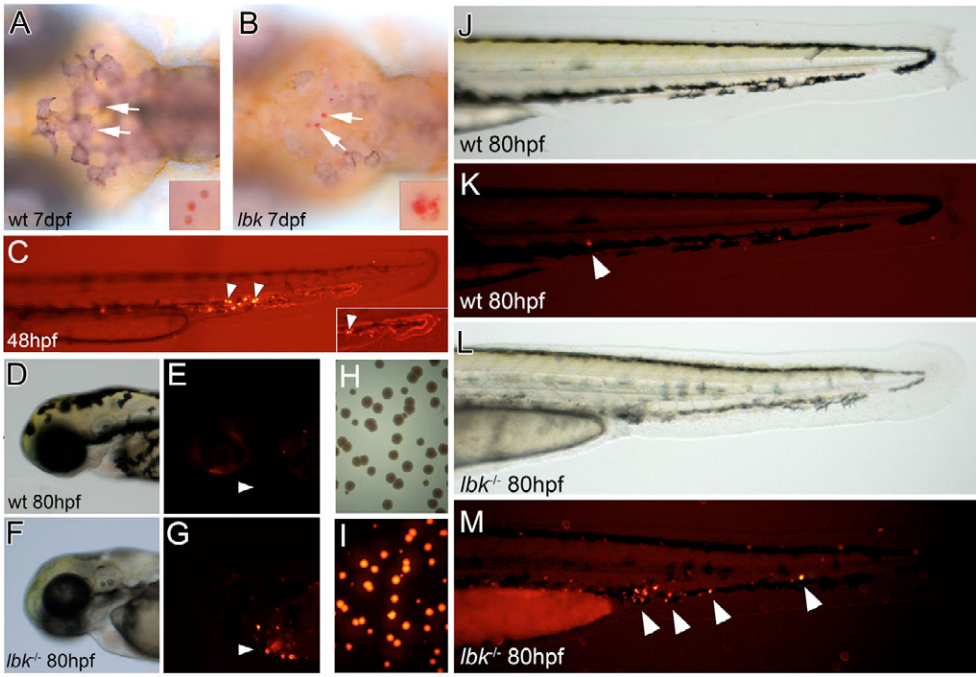

Fig. 5. *lbk* larvae show a compromised ability to clear bacterial infections. (**A**,**B**) Dorsal views of larvae in which macrophages were stained with Neutral Red to reveal intracellular vesicles (arrows). Compared with the vesicles observed in wild-type macrophages, those in *lbk* appear enlarged, heterogeneous in size and less regularly shaped. Insets show higher magnifications of macrophage vesicles. (**C**) Combined bright-field and fluorescence images of the tail of a 48 hpf larva 5 minutes after the injection of DsRed-fluorescent bacteria, showing bacteria still circulating in the bloodstream (inset; fluorescent traces of bacteria moving in blood vessels) and bacteria that have been engulfed by phagocytes (arrowheads). (**D-G**) Head regions of sibling and *lbk* larvae 32 hours after bacteria injection. Fluorescent bacteria-laden phagocytes are present in *lbk* (arrowheads). (**H**,**I**) Bright-field (H) and fluorescence images (I) of a bacterial plate showing bacterial colonies from an *lbk* larva macerated at 85 hpf, 37 hours after *Salmonella* injection. (**J-M**) Tails of sibling and *lbk* larvae 32 hours after bacteria injection. Arrowheads indicate fluorescent bacteria-containing phagocytes.

up until 5 dpf. Nonetheless, *lbk* larvae are severely visually impaired. Visual defects have also been reported for CHS and HPS syndromes (OMIM #214500; #203300). Interestingly, visual problems have not been diagnosed in individuals with GS to date (OMIM #214450; #607624; #609227). This may, however, be due to inconsistent testing of affected individuals or subsymptomatic reductions in visual acuity.

In addition to the RPE, there is also an accumulation of vesicles in hepatocytes and the cells lining the intestinal tract. These cells typically show high endo- and exocytic activities and large numbers of intracellular lysosomes and lysosome-related vesicles. The larger number of intracellular vesicles in the *lbk* liver and RPE is accompanied by an increase in overall liver and RPE size. As there is no apparent defect in the formation of vesicles but rather in their subsequent fusion (and hence recycling), it could be envisaged that the observed increase is due to an accumulation of vesicles, which in turn leads to an overall increase in cytoplasmic volume. An increase in liver volume (hepatomegaly) has also been described for individuals affected by CHS (OMIM #214500) and ARC syndrome (Gissen et al., 2004). Similarly, the intestinal phenotype observed in *lbk* is reminiscent of the granulomatous colitis described for individuals with HPS (OMIM #203300).

Defects in lysosome-related organelles might also be responsible for the immunological deficiencies observed in individuals with CHS and GS (Faigle et al., 1998; Griscelli et al., 1978). Macrophages, for instance, are crucial for the body's innate immune response. One of their key functions is the phagocytosis of pathogens. Pathogen-containing endosomes subsequently fuse with lysosomes and major histocompatibility complex class II (MHCII) compartments, a lysosome-related organelle, in which the pathogens are degraded and foreign peptides loaded onto MHCII complexes. Loaded MHCII complexes are subsequently delivered to the surface of macrophages for presentation to cells of the adaptive immune response. We found that *lbk* macrophages display an increase in intracellular vesicles, which might be indicative of a defect in the endosomal pathway and/or a defect in MHCII vesicle delivery to the plasma membrane. Importantly, our analyses show that the innate immune response to bacterial infection is significantly compromised in *lbk*.

ARC syndrome, CHS, GS and HPS are caused by defects in vesicle trafficking, particularly of lysosomes, lysosome-related organelles and late endosomes, and mutations in genes involved in vesicle transport, sorting, docking and fusion were shown to underlie these diseases. Moreover, ARC syndrome was demonstrated to be caused by mutations in the *vps33b* gene, a member of the HOPS complex, in humans (Gissen et al., 2004). Similarly, morpholino knock-down experiments targeting the zebrafish *vps33b* gene result in a phenotype resembling ARC syndrome (Matthews et al., 2005). Interestingly, the buff (*bf*) mouse, which harbours a mutation in the *Vps33a* gene, has been proposed as a model for HPS (Suzuki et al., 2003), suggesting a link between ARC syndrome and the CHS, GS and HPS group of diseases. The phenotypes observed in *lbk* encompass both symptoms observed in individuals with CHS, GS and HPS (liver, macrophage, hypopigmentation and visual phenotypes) and ARC syndrome (liver and intestinal phenotypes), providing further evidence for a link between these disorders.

Moreover, we have identified the gene mutated in *lbk* as *vam6*. Like Vps33p, the Vam6p protein is a component of the HOPS complex, which is required for SNARE complex assembly during vesicle docking and fusion. Mutations in the two alleles identified in this study lead to a premature STOP upstream of the CLH repeat domain and Ypt7p-interaction sequences, and the exchange of a highly conserved amino acid in the N-terminal CNH domain, respectively. The latter has been shown to be essential for lysosome clustering and fusion (Caplan et al., 2001). The Ypt7p-interaction domain mediates protein-protein interactions between Vam6p/Vps39p and Ypt7p/Rab7, a Rab-GTPase with essential functions in early to late endosome transport and late endosome-

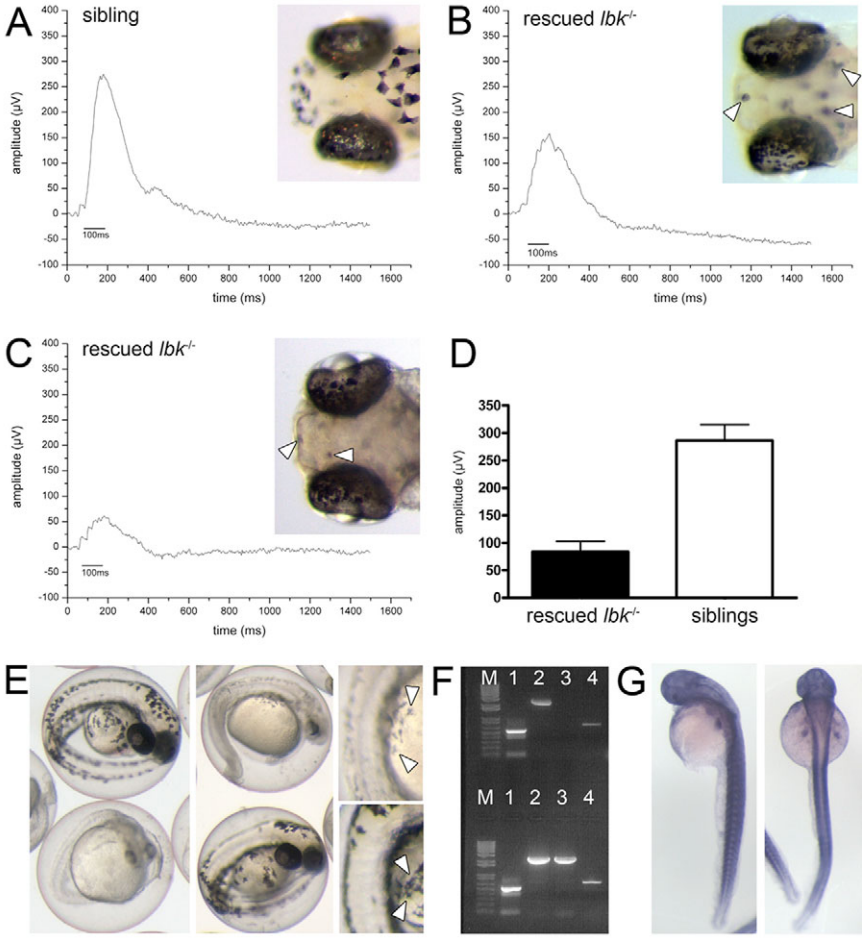

Fig. 6. The *lbk* phenotype can be partially rescued by the expression of *vam6* in *lbk*$^{-/-}$ larvae and phenocopied by *vam6* knock-down. (**A-C**) Electroretinogram analyses of 5 dpf *vam6* vector-injected and heat-shocked sibling (A) and *lbk*$^{-/-}$ (B,C) larvae. In contrast to uninjected *lbk* larvae (Fig. 3B), injected *lbk* larvae displayed significant b-waves, indicating partial rescue of retinal function. The b-wave amplitude varied between different *lbk* larvae with some showing up to 60% of the wild-type b-wave amplitude (B), while others reach only ~20% (C). Insets show head regions of *vam6* vector-injected sibling (A) and *lbk* larvae (B,C) and the extent of rescue in RPE and skin melanocyte pigmentation. Arrowheads indicate skin melanocytes with near wild-type levels of melanin in rescued larvae. (**D**) Quantification of the observed ERG rescue: sibling larvae display an average b-wave amplitude of 286 μV, *vam6* vector-injected *lbk* larvae show an average b-wave amplitude of 83 μV (n=7 for both sets of larvae; error bars show standard deviations). (**E**) Phenotype of the *vam6* knock-down at 36 hpf showing the hypopigmentation of the RPE and skin melanocytes (insets; arrowheads) characteristic of *lbk*. However, the knock-down results in additional phenotypes not observed in *lbk*, including a small head and eyes and a shortened body axis. Larvae displaying wild-type levels of melanin are age-matched control morpholino-injected individuals. (**F**) PCR analysis for the presence of *vam6* transcripts in RNA isolated from wild-type zebrafish zygotes (upper half of gel) and 24 hpf embryos (lower half). β-Actin (expressed at all developmental stages) and *pmel17* [onset of expression: ~20 hpf (Schonthaler et al., 2005)] served as controls. Lane M, 100 bp ladder; lane 1, amplification of a 530 bp β-actin cDNA fragment; lanes 2 and 4, amplification of two different fragments of the zebrafish *vam6* cDNA (2628 bp and 707 bp) with independent primer pairs; lane 3, amplification of a 2538 bp fragment of the *pmel17* cDNA. (**G**) Whole-mount in situ hybridisation on PTU-treated 48 hpf wild-type embryos (left, lateral view; right, dorsal view) showing *vam6* expression.

lysosome fusion, as well as in axonal retrograde transport (Deinhardt et al., 2006; Stein et al., 2003). It has been shown in yeast that Vam6p acts as a guanine nucleotide exchange factor for Ypt7p (Wurmser et al., 2000). When this exchange fails, Ypt7p is locked in its GDP-bound state and vesicle docking is blocked. This probably contributes to the vesicle phenotypes observed in *lbk*. In mammalian cells, both Rab7 and the HOPS complex are essential for the conversion of early into late endosomes (Rink et al., 2005). Interestingly, RNAi-mediated knock-down of Rab7 in HeLa cells leads to a cellular vesicle phenotype reminiscent of that observed in fibroblasts from individuals with CHS (Davies et al., 1997). Similarly, knock-down of RAB-7 in *C. elegans* leads to enlarged early and late endosomes and knock-down of HOPS complex members yield defects in gut lysosome formation (Poteryaev et al., 2007).

The next step in vesicle fusion, following the initial docking steps, is assembly of SNARE complexes. This process requires physical interactions between the HOPS complex and SNAREs (Collins et al., 2005; Price et al., 2000a; Price et al., 2000b; Sato et al., 2000). Mutations in Vam6p that abolish the functions of the CLH or CNH domains, respectively, might hamper these interactions and additionally contribute to the accumulation of vesicles in *lbk*.

The mutation in the *vam6* gene in *lbk* acts in a cell-autonomous fashion and affects cells derived from all three germ layers (skin melanocytes, RPE, PRCs in ectoderm; liver and intestine in endoderm; and macrophages in mesoderm). The most severe phenotypes are detected in cells that display high levels of phagocytic (RPE cells, macrophages) and secretory activity (hepatocytes, intestinal cells). Owing to the importance of vesicle trafficking in these cells, they are probably the first and most severely affected. The occurrence of only partially overlapping symptoms in ARC syndrome, CHS, GS and HPS, as well as the zebrafish *lbk* mutant could be due to the fact that lysosome-related organelles can be cell type-specific (Raposo and Marks, 2002) and thus defects in proteins required for these organelles might only affect certain cell types. The comparatively widespread organ dysfunction observed in *lbk* suggests that Vam6p is a core component with non-redundant functions in vesicle trafficking in a range of cell types.

It has recently been shown that a viral insertion disrupting the *vps18p* gene, another member of the HOPS complex, in zebrafish results in similar phenotypes as those observed in *lbk*, including a hypopigmentation of skin and RPE melanocytes, a lack of iridophore reflections, visual defects, hepatomegaly and an accumulation of vesicles in hepatocytes (Maldonado et al., 2006; Sadler et al., 2005). This provides further evidence for the importance of the HOPS complex in various cell types and organs.

In conclusion, the overlap in symptoms in human syndromes caused by defective lysosome trafficking and phenotypes observed in *lbk* suggest this mutant as a model for these inherited human

diseases and suggests a novel disease gene. Importantly, there is currently no mouse model for loss of function of Vam6p. Studies on *lbk* may offer important insights into the mechanisms underlying the observed symptoms and make these pathologies amenable to experimental manipulation.

The authors thank Matthew Harris for providing ENU-mutated zebrafish for the allele screen and for critically reading the manuscript; Annemarie Meijer for providing DsRed-expressing *Salmonella* and advice; Philippe Herbomel, Matthias Gesemann, Sarah Magee and Anne Spang for helpful discussions; Pawel Pasierbek for help with confocal LSM; Ines Gehring, Marianne Leißer and Brigitte Sailer for technical assistance; and John Vessey for critically reading the manuscript. This work was supported by an EMBO Long-term Fellowship (R.D.) and by the European Commission as part of the ZF-MODELS Integrated Project in the 6th Framework Programme, Contract No. LSHG-CT-2003-503496 (S.C.F.N., R.D. and R.G.).

Supplementary material

Supplementary material for this article is available at http://dev.biologists.org/cgi/content/full/135/2/387/DC1

References

Bajoghli, B., Aghaallaei, N., Heimbucher, T. and Czerny, T. (2004). An artificial promoter construct for heat-inducible misexpression during fish embryogenesis. *Dev. Biol.* **271**, 416-430.

Barak, Y. and Nir, E. (1987). Chediak-Higashi syndrome. *Am. J. Pediatr. Hematol. Oncol.* **9**, 42-55.

Bowers, K. and Stevens, T. H. (2005). Protein transport from the late Golgi to the vacuole in the yeast Saccharomyces cerevisiae. *Biochim. Biophys. Acta* **1744**, 438-454.

Brahmaraju, M., Shoeb, M., Laloraya, M. and Kumar, P. G. (2004). Spatio-temporal organization of Vam6P and SNAP on mouse spermatozoa and their involvement in sperm-zona pellucida interactions. *Biochem. Biophys. Res. Commun.* **318**, 148-155.

Brooks, D. A., Muller, V. J. and Hopwood, J. J. (2006). Stop-codon read-through for patients affected by a lysosomal storage disorder. *Trends Mol. Med.* **12**, 367-373.

Caplan, S., Hartnell, L. M., Aguilar, R. C., Naslavsky, N. and Bonifacino, J. S. (2001). Human Vam6p promotes lysosome clustering and fusion in vivo. *J. Cell Biol.* **154**, 109-122.

Clark, R. and Griffiths, G. M. (2003). Lytic granules, secretory lysosomes and disease. *Curr. Opin. Immunol.* **15**, 516-521.

Collins, K. M., Thorngren, N. L., Fratti, R. A. and Wickner, W. T. (2005). Sec17p and HOPS, in distinct SNARE complexes, mediate SNARE complex disruption or assembly for fusion. *EMBO J.* **24**, 1775-1786.

Dahm, R., Geisler, R. and Nüsslein-Volhard, C. (2005). Zebrafish (Danio rerio) genome and genetics. In *Encyclopedia of Molecular Cell Biology and Molecular Medicine*. Vol. 15 (ed. R. A. Meyers), pp. 593-626. Weinheim: Wiley-VCH.

Davies, J. P., Cotter, P. D. and Ioannou, Y. A. (1997). Cloning and mapping of human Rab7 and Rab9 cDNA sequences and identification of a Rab9 pseudogene. *Genomics* **41**, 131-134.

Deinhardt, K., Salinas, S., Verastegui, C., Watson, R., Worth, D., Hanrahan, S., Bucci, C. and Schiavo, G. (2006). Rab5 and Rab7 control endocytic sorting along the axonal retrograde transport pathway. *Neuron* **52**, 293-305.

Dell'Angelica, E. C. (2003). Melanosome biogenesis: shedding light on the origin of an obscure organelle. *Trends Cell Biol.* **13**, 503-506.

Faigle, W., Raposo, G., Tenza, D., Pinet, V., Vogt, A. B., Kropshofer, H., Fischer, A., de Saint-Basile, G. and Amigorena, S. (1998). Deficient peptide loading and MHC class II endosomal sorting in a human genetic immunodeficiency disease: the Chediak-Higashi syndrome. *J. Cell Biol.* **141**, 1121-1134.

Field, H. A., Ober, E. A., Roeser, T. and Stainier, D. Y. (2003). Formation of the digestive system in zebrafish. I. Liver morphogenesis. *Dev. Biol.* **253**, 279-290.

Geisler, R. (2002). Mapping and cloning. In *Zebrafish* (*Practical Approach Series*) (ed. C. Nusslein-Volhard and R. Dahm), pp. 175-212. Oxford: Oxford University Press.

Geisler, R., Rauch, G. J., Baier, H., van Bebber, F., Bross, L., Dekens, M. P., Finger, K., Fricke, C., Gates, M. A., Geiger, H. et al. (1999). A radiation hybrid map of the zebrafish genome. *Nat. Genet.* **23**, 86-89.

Gissen, P., Johnson, C. A., Morgan, N. V., Stapelbroek, J. M., Forshew, T., Cooper, W. N., McKiernan, P. J., Klomp, L. W., Morris, A. A., Wraith, J. E. et al. (2004). Mutations in VPS33B, encoding a regulator of SNARE-dependent membrane fusion, cause arthrogryposis-renal dysfunction-cholestasis (ARC) syndrome. *Nat. Genet.* **36**, 400-404.

Glass, A. S. and Dahm, R. (2004). The zebrafish as a model organism for eye development. *Ophthalmic Res.* **36**, 4-24.

Griscelli, C., Durandy, A., Guy-Grand, D., Daguillard, F., Herzog, C. and Prunieras, M. (1978). A syndrome associating partial albinism and immunodeficiency. *Am. J. Med.* **65**, 691-702.

Haffter, P., Granato, M., Brand, M., Mullins, M. C., Hammerschmidt, M., Kane, D. A., Odenthal, J., van Eeden, F. J., Jiang, Y. J., Heisenberg, C. P. et al. (1996). The identification of genes with unique and essential functions in the development of the zebrafish, Danio rerio. *Development* **123**, 1-36.

Herbomel, P., Thisse, B. and Thisse, C. (2001). Zebrafish early macrophages colonize cephalic mesenchyme and developing brain, retina, and epidermis through a M-CSF receptor-dependent invasive process. *Dev. Biol.* **238**, 274-288.

Hermansky, F., Cieslar, P., Matousova, O. and Smetana, K. (1975). Proceedings: study of albinism in relation to Hermansky-Pudlak syndrome. *Thromb. Diath. Haemorrh.* **34**, 360.

Ho, R. K. and Kane, D. A. (1990). Cell-autonomous action of zebrafish spt-1 mutation in specific mesodermal precursors. *Nature* **348**, 728-730.

Kelsh, R. N., Brand, M., Jiang, Y. J., Heisenberg, C. P., Lin, S., Haffter, P., Odenthal, J., Mullins, M. C., van Eeden, F. J., Furutani-Seiki, M. et al. (1996). Zebrafish pigmentation mutations and the processes of neural crest development. *Development* **123**, 369-389.

Kimmel, C. B., Ballard, W. W., Kimmel, S. R., Ullmann, B. and Schilling, T. F. (1995). Stages of embryonic development of the zebrafish. *Dev. Dyn.* **203**, 253-310.

Knapik, E. W., Goodman, A., Ekker, M., Chevrette, M., Delgado, J., Neuhauss, S., Shimoda, N., Driever, W., Fishman, M. C. and Jacob, H. J. (1998). A microsatellite genetic linkage map for zebrafish (Danio rerio). *Nat. Genet.* **18**, 338-343.

Makhankov, Y. V., Rinner, O. and Neuhauss, S. C. (2004). An inexpensive device for non-invasive electroretinography in small aquatic vertebrates. *J. Neurosci. Methods* **135**, 205-210.

Maldonado, E., Hernandez, F., Lozano, C., Castro, M. E. and Navarro, R. E. (2006). The zebrafish mutant vps18 as a model for vesicle-traffic related hypopigmentation diseases. *Pigment Cell Res.* **19**, 315-326.

Matthews, R. P., Plumb-Rudewiez, N., Lorent, K., Gissen, P., Johnson, C. A., Lemaigre, F. and Pack, M. (2005). Zebrafish vps33b, an ortholog of the gene responsible for human arthrogryposis-renal dysfunction-cholestasis syndrome, regulates biliary development downstream of the onecut transcription factor hnf6. *Development* **132**, 5295-5306.

Morrison, R. L. and Frost-Mason, S. K. (1991). Ultrastructural analysis of iridophore organellogenesis in a lizard, Sceloporus graciosus (Reptilia: Phrynosomatidae). *J. Morphol.* **209**, 229-239.

Nakamura, N., Hirata, A., Ohsumi, Y. and Wada, Y. (1997). Vam2/Vps41p and Vam6/Vps39p are components of a protein complex on the vacuolar membranes and involved in the vacuolar assembly in the yeast Saccharomyces cerevisiae. *J. Biol. Chem.* **272**, 11344-11349.

Poteryaev, D., Fares, H., Bowerman, B. and Spang, A. (2007). Caenorhabditis elegans SAND-1 is essential for RAB-7 function in endosomal traffic. *EMBO J.* **26**, 301-312.

Price, A., Seals, D., Wickner, W. and Ungermann, C. (2000a). The docking stage of yeast vacuole fusion requires the transfer of proteins from a cis-SNARE complex to a Rab/Ypt protein. *J. Cell Biol.* **148**, 1231-1238.

Price, A., Wickner, W. and Ungermann, C. (2000b). Proteins needed for vesicle budding from the Golgi complex are also required for the docking step of homotypic vacuole fusion. *J. Cell Biol.* **148**, 1223-1229.

Raposo, G. and Marks, M. S. (2002). The dark side of lysosome-related organelles: specialization of the endocytic pathway for melanosome biogenesis. *Traffic* **3**, 237-248.

Rieder, S. E. and Emr, S. D. (1997). A novel RING finger protein complex essential for a late step in protein transport to the yeast vacuole. *Mol. Biol. Cell* **8**, 2307-2327.

Rink, J., Ghigo, E., Kalaidzidis, Y. and Zerial, M. (2005). Rab conversion as a mechanism of progression from early to late endosomes. *Cell* **122**, 735-749.

Rinner, O., Makhankov, Y. V., Biehlmaier, O. and Neuhauss, S. C. (2005a). Knockdown of cone-specific kinase GRK7 in larval zebrafish leads to impaired cone response recovery and delayed dark adaptation. *Neuron* **47**, 231-242.

Rinner, O., Rick, J. M. and Neuhauss, S. C. (2005b). Contrast sensitivity, spatial and temporal tuning of the larval zebrafish optokinetic response. *Invest. Ophthalmol. Vis. Sci.* **46**, 137-142.

Sadler, K. C., Amsterdam, A., Soroka, C., Boyer, J. and Hopkins, N. (2005). A genetic screen in zebrafish identifies the mutants vps18, nf2 and foie gras as models of liver disease. *Development* **132**, 3561-3572.

Sato, T. K., Rehling, P., Peterson, M. R. and Emr, S. D. (2000). Class C Vps protein complex regulates vacuolar SNARE pairing and is required for vesicle docking/fusion. *Mol. Cell* **6**, 661-671.

Schonthaler, H. B., Lampert, J. M., von Lintig, J., Schwarz, H., Geisler, R. and Neuhauss, S. C. (2005). A mutation in the silver gene leads to defects in melanosome biogenesis and alterations in the visual system in the zebrafish mutant fading vision. *Dev. Biol.* **284**, 421-436.

Seals, D. F., Eitzen, G., Margolis, N., Wickner, W. T. and Price, A. (2000). A Ypt/Rab effector complex containing the Sec1 homolog Vps33p is required for homotypic vacuole fusion. *Proc. Natl. Acad. Sci. USA* **97**, 9402-9407.

Stein, M. P., Dong, J. and Wandinger-Ness, A. (2003). Rab proteins and endocytic trafficking: potential targets for therapeutic intervention. *Adv. Drug Deliv. Rev.* **55**, 1421-1437.

Stinchcombe, J., Bossi, G. and Griffiths, G. M. (2004). Linking albinism and immunity: the secrets of secretory lysosomes. *Science* **305**, 55-59.
Stroupe, C., Collins, K. M., Fratti, R. A. and Wickner, W. (2006). Purification of active HOPS complex reveals its affinities for phosphoinositides and the SNARE Vam7p. *EMBO J.* **25**, 1579-1589.
Suzuki, T., Oiso, N., Gautam, R., Novak, E. K., Panthier, J. J., Suprabha, P. G., Vida, T., Swank, R. T. and Spritz, R. A. (2003). The mouse organellar biogenesis mutant buff results from a mutation in Vps33a, a homologue of yeast vps33 and Drosophila carnation. *Proc. Natl. Acad. Sci. USA* **100**, 1146-1150.
van der Sar, A. M., Musters, R. J., van Eeden, F. J., Appelmelk, B. J., Vandenbroucke-Grauls, C. M. and Bitter, W. (2003). Zebrafish embryos as a model host for the real time analysis of Salmonella typhimurium infections. *Cell. Microbiol.* **5**, 601-611.
van der Sar, A. M., Stockhammer, O. W., van der Laan, C., Spaink, H. P., Bitter, W. and Meijer, A. H. (2006). MyD88 innate immune function in a zebrafish embryo infection model. *Infect. Immun.* **74**, 2436-2441.
Wurmser, A. E., Sato, T. K. and Emr, S. D. (2000). New component of the vacuolar class C-Vps complex couples nucleotide exchange on the Ypt7 GTPase to SNARE-dependent docking and fusion. *J. Cell Biol.* **151**, 551-562.